

# $H_\infty$ Current Controller of WRIM Based Flywheel Storage System under Unbalanced Stator Voltage

Ahmed Lazrak<sup>\*‡</sup>, Ahmed Abbou<sup>\*</sup>

<sup>\*</sup> Department of Electrical Engineering, Mohammadia School of Engineering, Mohammed V University, Agdal Rabat 10090, Morocco

(lazrak.ahmedd@gmail.com, abbou@emi.ac.ma)

<sup>‡</sup> Corresponding Author; Ahmed Lazrak, Agadir 80000 Morocco, Tel: +212677335096, lazrak.ahmedd@gmail.com

*Received: 14.02.2019 Accepted: 25.03.2019*

**Abstract-** Flywheel storage systems (FSSs) are commonly associated with wind farms to support them to provide services to the grid such as power smoothing, frequency control, and voltage control. Although FSSs are not concerned by the grid code requirements, their stability and availability under unbalanced stator voltages are very important to ensure both wind farm stability and supply quality. In this context, this paper proposes a robust  $H_\infty$  controller for wound rotor induction machine (WRIM) driven FSS under stator voltage unbalance. The controller purpose is to suppress rotor current oscillations resulting from the negative sequence as well as to guarantee the system robustness in the presence of parameter uncertainties. The robust controller design based on mixed-sensitivity  $H_\infty$  control that guarantees the robust stability (RS) and robust performance (RP) is presented in detail. The performance of the  $H_\infty$  controller has been evaluated with simulations in MATLAB/Simulink using slip power systems for both unbalanced stator voltage and parameter uncertainties.

**Keywords** Flywheel storage system, wound rotor induction machine, wind farm, unbalanced stator voltage,  $H_\infty$  control.

## 1. Introduction

Flywheel storage systems (FSSs) are commonly associated with wind farms to support them to provide services to the grid such as power smoothing, voltage control, frequency control, and low voltage ride-through capability [1-6].

Among all energy storage systems, FSS has gained increasing attention in wind power due to their advantages. First, they can interchange medium to large powers (above MW) during short periods with faster dynamic response. Second, they provide high number of charge discharge cycles. Flywheels are also characterized by higher energy efficiency, long life time, no pollution, and low maintenance requirement [7].

Considering the development of the FSSs over the last decade, several machine types were applied such as Induction Machine (IM) [2-4], Permanent Magnet Synchronous Machine (PMSM) [5], switched reluctance machine (SRM) [8], Synchronous homopolar machine (SHM) [9], Brushless direct current machine (BLDMC) [10], and Synchronous reluctance machine [11].

Research into Wound Rotor Induction Machine (WRIM) for FSSs is motivated by the fact that the converters can be designed with a modest cost [12-17]. This is because the converters rating is typically 30% ~ 35% of system power, while the rotor speed variation is in the range of +33% of the synchronous speed [18]. In addition, the WRIM with bidirectional converters in the rotor circuit enables the decoupling control of active and reactive power [18-21]. The common control techniques for WRIM based FSS are mainly based on the dq rotating frame decoupling and the vector control [15-17].

FSSs as an integrated part of wind farms are usually located in remote and rural areas. The electric grid in these places is usually weak and unbalanced stator voltages can occur [22]. Therefore, the WRIM based FSS can be subjected to high unbalanced rotor currents even under small unbalanced stator voltages [22]. Without appropriate control, this can lead to the burning of the electrical machine and the converters. As for wind farms, FSSs might have to be disconnected from the electric grid to protect themselves from rotor over currents. Various control strategies were proposed to enhance the dynamic operation of WRIM under

unbalanced stator voltages for wind power applications [22-29].

In [22], independent positive and negative sequence control are proposed based on a symmetrical component theory. However, this approach will reduce the system's dynamic response and stability, due to the errors and time delay introduced by the positive and the negative sequence decomposition [23]. To overcome these problems, an improved control schemes for DFIG based wind turbine under unbalanced condition were proposed in [23]. The idea is to combine a PI controller with a resonant regulator R tuned at twice the line frequency. In this way, a PIR regulator in the positive synchronous reference frame is used to regulate directly the positive and negative sequence component of the rotor currents.

Nevertheless, the PIR controller remains valid only for the nominal model which is usually simplified as a first order system [23]. Thus, the system robust stability (RS) under parameters uncertainties is not considered. Therefore, the stability and robustness for a non-nominal model cannot be assured. Other methods such as direct power control (DPC) [24,25], predictive current control strategy [26], predictive direct power control [27], and sliding-mode control combined with DPC [28], have been used in DFIG control system under unbalanced grid conditions. However, parameters uncertainties are not fully considered.

In robust control theory,  $H_\infty$  control is a powerful technique to synthesize controllers achieving robust stability and robust performance for systems under conditions of uncertainty and disturbances [30,31]. Among all the  $H_\infty$  techniques for controller design, Glover and McFarlane proposed the  $H_\infty$  loop shaping synthesis which combines the  $H_\infty$  robust stabilization using normalized coprime factorization with the classical loop shaping [32]. The main idea is to shape the open loop singular values by pre and post-filters, and the resulting shaped model is then stabilized using  $H_\infty$  control [32]. An alternative to  $H_\infty$  loop shaping synthesis is the mixed-sensitivity  $H_\infty$  control. In this method,  $H_\infty$  optimization is used to shape sensitivity function S along with other closed-loop transfer functions such as the complementary sensitivity function T [34].

Some studies related to WRIM  $H_\infty$  control are discussed below. In [30],  $H_\infty$  damping current controller is employed for DFIG based wind farm to effectively mitigate sub-synchronous control interactions with series compensated grid lines. In [31],  $H_\infty$  controllers are designed to control the rotor currents of DFIG based wind turbine under harmonic grid voltage and parameter perturbation. The  $H_\infty$  controllers for load mitigation in wind turbine based DFIG are proposed in [35]. In [36], the  $H_\infty$  control is developed to control independently the stator voltage and frequency of DFIG for stand-alone applications.

Considering the benefits of FSSs for wind farms, their stability and availability under unbalanced stator voltages are very important. Although FSSs are not concerned by the grid code requirements, they must remain connected to the grid

during unbalanced stator voltage to ensure both wind farm stability and supply quality.

The main contribution of this work is to develop a robust  $H_\infty$  controller for WRIM based FSS in order to suppress rotor currents oscillations resulting from negative sequence, and guarantee the system RS and RP under unbalanced stator voltage with parameter uncertainties.

This work proposes a worst case operation scenario, where the proposed  $H_\infty$  controller design takes the grid disturbance, speed variation and parameter perturbation into account. First, Section II analyses the influence of unbalanced stator voltage and parameter uncertainties on the rotor currents based on an uncertain model of the WRIM. Next, the  $H_\infty$  controller design based on mixed-sensitivity  $H_\infty$  control, and the weights selection are detailed in Section III. Finally, comparative simulation results are presented in Section IV to demonstrate the effectiveness and the robustness of the proposed  $H_\infty$  controller under unbalanced stator voltage with parameter uncertainties, followed by a conclusion in Section V.

## 2. Uncertain Model of WRIM Based Flywheel Storage System

### 2.1 System Overview

The flywheel storage system is modeled as a WRIM coupled with a mechanical flywheel which stores the electrical energy in kinetic energy form. Figure 1 shows a flywheel storage system integrating a WRIM for wind power smoothing. The FSS can absorb or generate power via the WRIM and converters, in order to smooth the power variation of the wind farm.

### 2.2 WRIM based Flywheel Storage System Modelling

The energy stored in the flywheel system is proportional to its inertia  $J_f$  and the speed variation of the WRIM  $\omega_{rf}$  as shown in Eq. (1):

$$E_f = \frac{1}{2} J_f \omega_{rf}^2 \quad (1)$$

For wind power smoothing, the kinetic energy of the WRIM is determined by [16]:

$$E_f = \int P_f dt = \int (P_g - P_w) dt \quad (2)$$

Where,  $P_g$  is the desired grid power,  $P_w$  is the optimal wind power, and  $P_f$  is the reference active power exchanged between the flywheel storage system and the power grid.

The dynamic model of WRIM in the synchronous rotating reference frame can be defined as [37]:

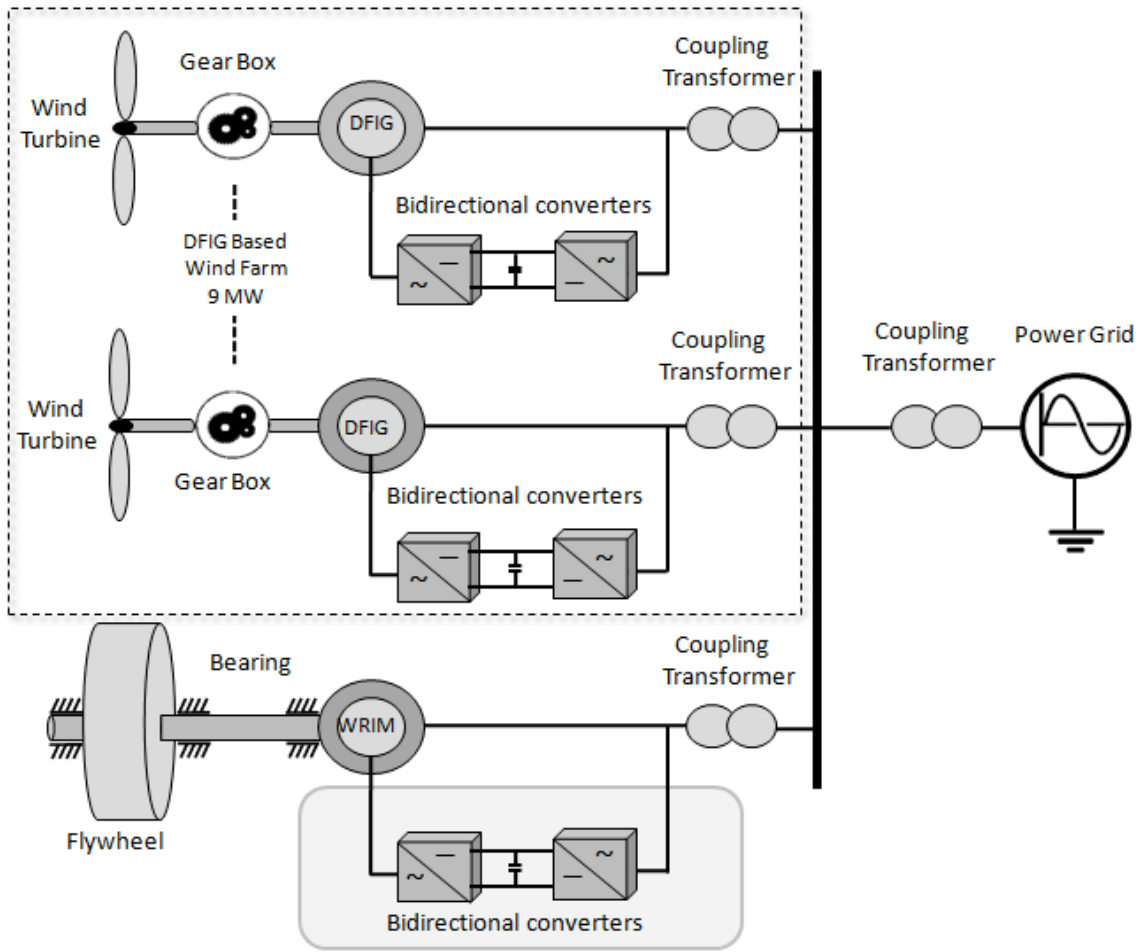


Fig. 1. Flywheel storage system based WRIM used for wind farm power smoothing

$$\left\{ \begin{aligned}
 u_{dsf} &= R_s i_{dsf} + \frac{d\varphi_{dsf}}{dt} - w_{sf} \varphi_{qsf} \\
 u_{qsf} &= R_s i_{qsf} + \frac{d\varphi_{qsf}}{dt} + w_{sf} \varphi_{dsf} \\
 u_{drf} &= R_r i_{drf} + \frac{d\varphi_{drf}}{dt} - (w_{sf} - w_{rf}) \varphi_{qrf} \\
 u_{qrf} &= R_r i_{qrf} + \frac{d\varphi_{qrf}}{dt} + (w_{sf} - w_{rf}) \varphi_{drf} \\
 \varphi_{dsf} &= L_s i_{dsf} + L_m i_{drf} \\
 \varphi_{qsf} &= L_s i_{qsf} + L_m i_{qrf} \\
 \varphi_{drf} &= L_r i_{drf} + L_m i_{dsf} \\
 \varphi_{qrf} &= L_r i_{qrf} + L_m i_{qsf}
 \end{aligned} \right. \quad (3)$$

Where the subscripts “d” and “q” represent the Park components,  $R_s$  and  $R_r$  are resistances of the stator and rotor,  $L_{\sigma s}$  and  $L_{\sigma r}$  are the stator and rotor leakage inductances,  $L_m$  is the mutual inductance,  $L_s = L_{\sigma s} + L_m$  and  $L_r = L_{\sigma r} + L_m$  are the stator and rotor winding total self-inductances,  $\varphi_{dsf}$  and  $\varphi_{qsf}$  are the stator magnetic flux linkages,  $\varphi_{drf}$  and  $\varphi_{qrf}$  are the rotor flux linkages,  $u_{dsf}$  and  $u_{qsf}$  are the stator voltages,  $u_{drf}$

and  $u_{qrf}$  are the rotor voltages,  $i_{dsf}$  and  $i_{qsf}$  are the stator currents,  $i_{drf}$  and  $i_{qrf}$  are the rotor currents,  $w_{sf}$  is the synchronous angular speed, and  $w_{rf}$  is the rotor angular speed.

The control of WRIM driven FSS can be conveniently analyzed by the stator flux orientation control with Park transformations [37]. Since our purpose in this work is protecting the WRIM and the converters under unbalanced stator voltage, the FSS model will focus on the rotor currents control. Based on Eq. (3), the WRIM model can be described by the state-space form given in Eq. (4).

$$\begin{cases}
 \dot{x} = Ax + Bu + B_d d \\
 y = Cx + Du
 \end{cases} \quad (4)$$

Where, the state vectors consist of stator and rotor currents  $x = [i_{dsf} \ i_{qsf} \ i_{drf} \ i_{qrf}]$ , the outputs consist of the rotor currents  $y = [i_{drf} \ i_{qrf}]$ . The WRIM is controlled by the rotor side converter. Thus  $u = [u_{drf} \ u_{qrf}]$  is the input vector, and the stator voltage  $d = [u_{dsf} \ u_{qsf}]$  is

considered as a disturbance input vector that perturbs the rotor currents.

The system in Eq. (4) can be expressed in transfer function terms as,

$$y = G(s)u + G_d(s)d \quad (5)$$

Where  $G(s) = C(sI - A)^{-1}B$  and  $G_d(s) = C(sI - A)^{-1}B_d$  represent the plant and the disturbances respectively. All the system parameters used in this work are given in Table 1, and the parameter matrices are,

$$A = \begin{bmatrix} a_{11} & a_{12} & a_{13} & a_{14} \\ a_{21} & a_{22} & a_{23} & a_{24} \\ a_{31} & a_{32} & a_{33} & a_{34} \\ a_{41} & a_{42} & a_{43} & a_{44} \end{bmatrix} \quad B = \frac{1}{L_m^2 - L_s L_r} \begin{bmatrix} L_m & 0 \\ 0 & L_m \\ -L_s & 0 \\ 0 & -L_s \end{bmatrix}$$

$$B_d = \frac{1}{L_m^2 - L_s L_r} \begin{bmatrix} -L_r & 0 \\ 0 & -L_r \\ L_m & 0 \\ 0 & L_m \end{bmatrix} \quad C = \begin{bmatrix} 0 & 0 & 1 & 0 \\ 0 & 0 & 0 & 1 \end{bmatrix} \quad D = 0$$

Where  $a_{11} = \frac{L_r R_s}{L_m^2 - L_s L_r}$ ,  $a_{12} = \frac{L_m^2 w_{slip} - L_s L_r w_{sf}}{L_m^2 - L_s L_r}$ ,  $a_{22} = a_{11}$

$a_{13} = \frac{-L_m R_r}{L_m^2 - L_s L_r}$ ,  $a_{14} = \frac{-L_m L_r w_{rf}}{L_m^2 - L_s L_r}$ ,  $a_{23} = -a_{14}$ ,  $a_{24} = a_{13}$

$a_{21} = \frac{-L_m^2 w_{slip} + L_s L_r w_{sf}}{L_m^2 - L_s L_r}$ ,  $a_{31} = \frac{-L_m R_s}{L_m^2 - L_s L_r}$ ,  $a_{42} = a_{31}$

$a_{32} = \frac{L_m L_s w_{rf}}{L_m^2 - L_s L_r}$ ,  $a_{33} = \frac{L_s R_r}{L_m^2 - L_s L_r}$ ,  $a_{34} = \frac{L_m^2 w_{sf} - L_s L_r w_{slip}}{L_m^2 - L_s L_r}$

$a_{41} = -a_{32}$ , and  $a_{44} = a_{33}$

**Table 1.** (a) Parameters of the WRIM based FSS. (b) Parameters of the DFIG based wind farm.

(b)	
Radius of the wind	32.25 m
Gain multiplier	90
Air density	1.225 Kg/ m <sup>3</sup>
Inertia	1000 Kg. m <sup>2</sup>
Viscous torque	0.0024
Stator resistance	0.012 Ω
Rotor resistance	0.021 Ω
Stator inductance	0.0137 H
Rotor inductance	0.0136 H
Magnetizing inductance	0.0135 H
Number of pole pairs	2
Rated power	6×1.5 MW

### 2.3 Uncertain Model of WRIM based FSS

The uncertain state-space model of WRIM can be described as:

$$\begin{cases} \dot{x} = (A + \delta_A)x + (B + \delta_B)u + (B_d + \delta_{B_d})d \\ y = Cx + Du \end{cases} \quad (6)$$

Where,  $\delta_A$ ,  $\delta_B$  and  $\delta_{B_d}$  define the uncertain part of the matrices  $A$ ,  $B$ , and  $C$  respectively, and the uncertainty range of  $R_r$ ,  $L_m$ ,  $L_{\sigma s}$  and  $L_{\sigma r}$  is  $\pm 50\%$ .

The uncertainty of wind power is reflected as the change of speed. The rotor speed variation is usually in the range of  $\pm 33\%$  of the synchronous speed.

The frequency characteristics of the uncertain WRIM model based on Eq. (3) are shown in Fig.2 and Fig.3. These two figures show the bode plots from  $u_{dsf}$  to  $i_{drf}$  considering parameter perturbation and speed variation. The nominal model is shown by the curve marked with 'x', and other curves represent the uncertain models.

It is shown that the frequency characteristics of  $i_{drf}$  have a range of variations with different uncertain parameters and different speed, indicating that the stator voltage disturbance and the WRIM parameter perturbation can influence the rotor currents control.

### 3. H<sub>∞</sub> Controller Design

The schematic diagram for the control of the flywheel storage system under unbalanced stator voltage is designed as a cascaded structure as shown in Fig.4. The H<sub>∞</sub> controller is employed in the rotor current loop, while the outer control loop adopts a classical PI controller.

(a)	
Grid frequency	50 Hz
Nominal speed	1500 rpm
Stator voltage	690 V
Number of pole pairs	2
Stator resistance	0.0026 Ω
Rotor resistance	0.0029 Ω
Mutual inductance	0.0025 H
Stator inductance	0.0026 H
Rotor inductance	0.0026 H
Inertia	127 Kg. m <sup>2</sup>
Rated power	2 MW

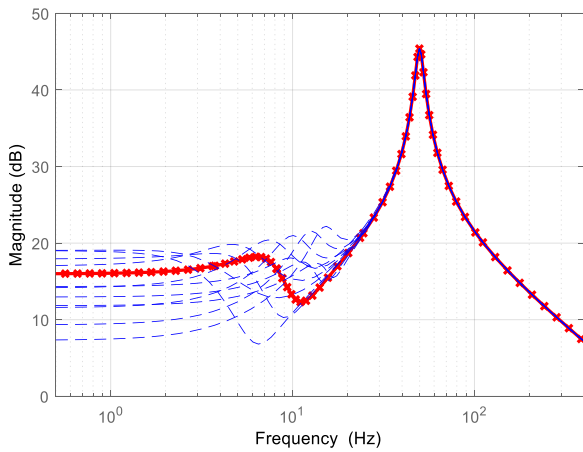


Fig. 2. Bode plot of the uncertain plant from  $u_{dsf}$  to  $i_{drf}$  with rotor speed variation

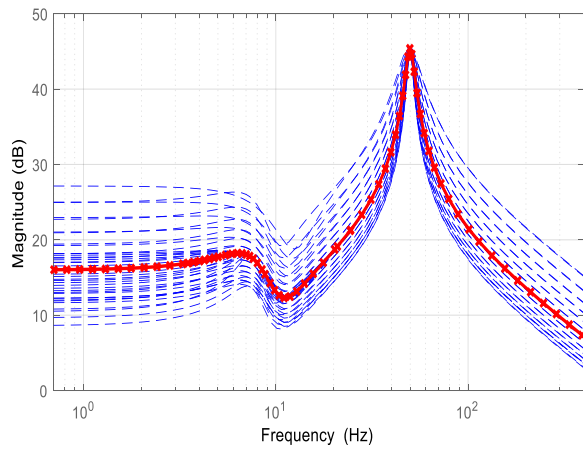


Fig. 3. Bode plot of the uncertain plant from  $u_{dsf}$  to  $i_{drf}$  with parameters uncertainty

3.1  $H_\infty$  mixed-sensitivity design

We will consider the  $H_\infty$  mixed-sensitivity design problem illustrated in Fig.5 [30], [34]. It can be viewed as a tracking problem, but with an additional uncertainty weight  $W_0$ . For the purposes of design, the stator voltage  $d = [u_{dsf} \quad u_{qsf}]^T$  is modelled as a disturbance that perturbs the rotor current outputs. So, the disturbance  $G_d$  is included as an extra input to the standard  $H_\infty$  mixed sensitivity design.

The parameter uncertainty is presented by unstructured multiplicative output uncertainties  $\Delta$  satisfying  $\|\Delta\|_\infty \leq 1$ , with a weight  $W_0$  using  $G_p = (I + W_0\Delta)G$ , where  $G$  is the nominal model and  $G_p$  present the uncertain model [34].  $u_\Delta$  and  $y_\Delta$  are the output and input vectors of  $\Delta$ , respectively.  $w$  and  $z$  present the exogenous inputs and the weighted outputs, respectively.

The shaped generalized plant  $P$  which has the inputs  $[u_\Delta \quad w \quad u]^T$  and outputs  $[y_\Delta \quad z \quad v]^T$  can be derived as [30], [34]:

$$\begin{bmatrix} y_\Delta \\ z \\ v \end{bmatrix} = \begin{bmatrix} P_{11} & P_{12} \\ P_{21} & P_{22} \end{bmatrix} \begin{bmatrix} u_\Delta \\ w \\ u \end{bmatrix} \quad (7)$$

Where,  $P_{11} = \begin{bmatrix} 0 & 0 & G_d W_0 \\ 0 & 0 & 0 \\ -W_1 & W_1 & -W_1 G_d \end{bmatrix}$ ,  $P_{12} = \begin{bmatrix} G W_0 \\ W_2 \\ -W_1 G \end{bmatrix}$ ,  
 $P_{21} = [-I \quad I \quad -G_d]$ , and  $P_{22} = -G$

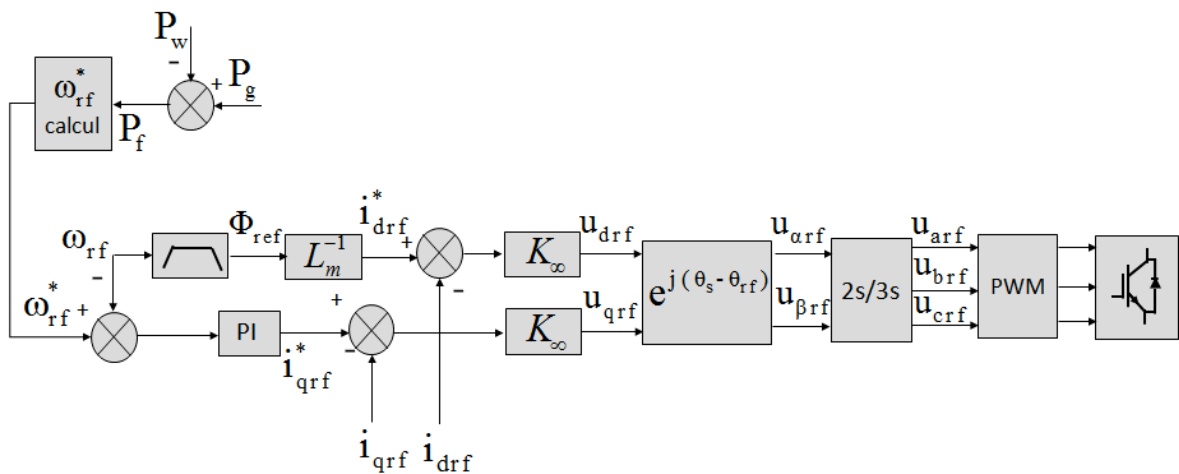


Fig. 4. Structure of the robust control scheme for WRIM based FSS under unbalanced stator voltage

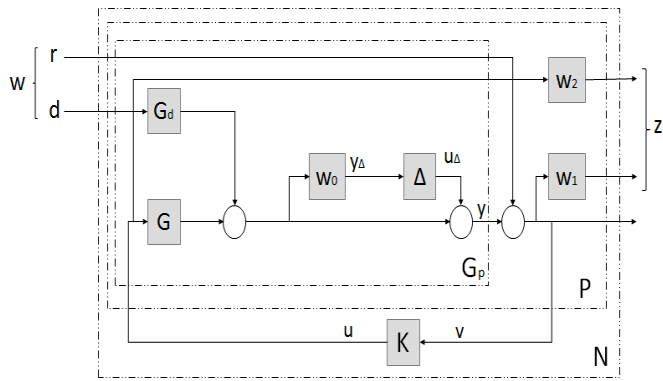


Fig. 5.  $H_\infty$  mixed sensitivity design

Next, the lower linear fractional transformation  $F_l(P, K)$  is used to derive the system  $N$  as expressed in Eq. (8).

$$N = \begin{bmatrix} -GW_0KS & GW_0KS & G_dW_0 - GW_0KSG_d \\ -W_2KS & W_2KS & -W_2KSG_d \\ W_1(GKS - I) & W_1(I - GKS) & W_1(GKS - I)G_d \end{bmatrix} \quad (8)$$

Where  $N = F_l(P, K) = P_{11} + P_{12}K(I - P_{22}K)^{-1}P_{21}$

The objective is to find a stabilizing controller  $K$  which based on the information in  $v$ , generates an input  $u$  which minimizes the influence of  $w$  on  $z$ , and therefore minimizes the  $H_\infty$  norm of the closed-loop transfer function  $N$ .

$$\|N\|_\infty = \gamma_{\min} < \gamma \quad (9)$$

The value of  $\gamma_{\min}$  is obtained using the algorithm of Doyle and by reducing  $\gamma$  iteratively [38].

### 3.2 The Weights Selection

Multiplicative output uncertainty is often used in robust control to lump several sources of uncertainty into a single perturbation. Consider the relative errors of possible perturbed plants  $G_p$  resulting from parametric uncertainty presented as multiplicative output uncertainty [34]:

$$l_0(j\omega) = \max_w \bar{\sigma} \left( \frac{G_p(j\omega) - G(j\omega)}{G(j\omega)} \right) \quad (10)$$

The objective is to find a weighting function  $W_0$  that can cover the maximum magnitude of all relative error curves for all frequencies:

$$|W_0(j\omega)| \geq l_0(j\omega) \quad (11)$$

The inequality in Eq. (1) is satisfied by using a low order filter:

$$W_0 = \frac{\tau s + r_0}{(\tau / r_\infty)s + 1} \quad (12)$$

Where  $r_0$  is the relative uncertainty at steady state,  $1/\tau$  is the frequency at which the relative uncertainty reaches 100% and  $r_\infty$  is the magnitude of the weight at high frequency.

Figure 6 illustrates the singular value curves of relative errors and the weight  $W_0$ , showing that the maximum magnitude of all possible curves of  $\sigma \left( \frac{G_p(j\omega) - G(j\omega)}{G(j\omega)} \right)$  is below  $\sigma(W_0)$  for all frequencies.

In order to track the low-frequency reference signal instead of high-frequency noises, and to guarantee the 2<sup>nd</sup> order harmonic suppression, a higher-order weight is applied to the tracking error  $v$ :

$$W_1 = \frac{\left( \frac{s}{M_1^{0.5}} + w_1 \right)^2}{(s + w_1 A_1^{0.5})^2} + \frac{k w_r s}{s^2 + 2\xi w_r s + w_r^2} \quad (13)$$

Where  $|W_1(j\omega)|^{-1}$  is equal to  $A_1 \leq 1$  at low frequencies, and equal to  $M_1 \geq 1$  at high frequencies.  $k$ ,  $\xi$ , and  $w_r$  are the gain ratio, the damping ratio, and the resonance frequency of the band-pass filter, respectively.

A first-order high-pass filter is used to limit the closed-loop bandwidth with a low frequency gain of approximately -60 dB to ensure that the cost function in Eq. (9) is dominated by  $W_1$  at low frequencies.

$$W_2 = \frac{s}{s + w_2 A_2} \quad (14)$$

The parameters of the weights  $W_0$ ,  $W_1$ , and  $W_2$  are listed in Table 2.

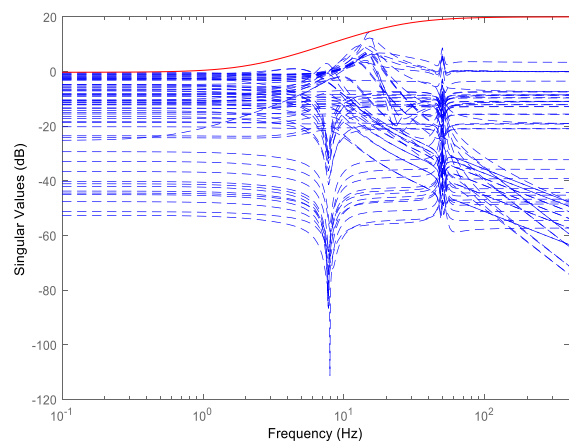


Fig. 6. Relative errors and the weight  $W_0$

### 3.3 The robust stability (RS) and robust performance (RP) validation

The resulting  $H_\infty$  controller is analyzed to verify if the RS is satisfied and the system remains stable for all

perturbed models. The requirement of robust stability (RS) in the case of system with multiplicative output uncertainty gives an upper bound on the closed-loop system  $T$  [34]:

$$\|T\|_{\infty} < \left\| \frac{1}{W_0} \right\|_{\infty} \quad (15)$$

If the design is not robust, the parameters of the weights will need to be modified until RS is satisfied.

The singular values of  $1/W_0$  and the uncertain closed-loop system  $T$  resulting from parametric uncertainty are shown in Fig.7. It is seen that  $1/W_0$  can cover the maximum of all the amplitude-frequency curves of  $T$  satisfying the RS requirement in Eq. (15).

Since the RS requirement is validated, we will then analyze the resulting  $H_{\infty}$  controller to see if the RP is satisfied. Thus, the performance specifications are analyzed by considering all perturbed plants, and requiring that even the worst case of perturbed model satisfies the performance specifications. The condition for robust performance with multiplicative output uncertainty is given in Eq. (16) [34]:

$$\|W_1 S\|_{\infty} + \|W_0 T\|_{\infty} < 1 \quad (16)$$

The curves of the RP are shown in Fig. 8. All the values of  $\|W_1 S\|_{\infty} + \|W_0 T\|_{\infty}$  are below 1 satisfying the RP requirement in Eq. (16).

**Table 2.** Parameters of the weights  $W_0$ ,  $W_1$ , and  $W_2$

$W_0$	
$\tau$	0.02
$r_0$	0.967
$r_{\infty}$	10
$W_1$	
$A_1$	1
$M_1$	20
$w_1$	60
$k$	0.01
$w_r$	$200\pi$
$\zeta$	0.01
$W_2$	
$A_2$	$12 \cdot 10^6$
$M_2$	20
$w_2$	$5 \cdot 10^{-6}$

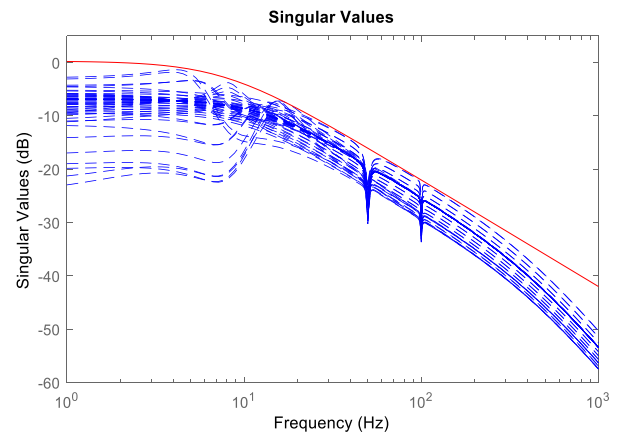


**Fig. 7.** Robust stability (RS) analysis

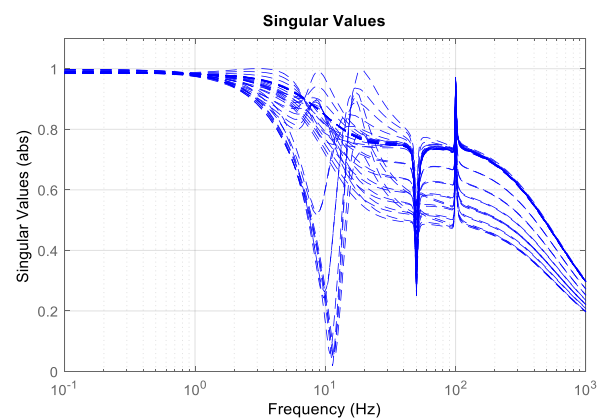


**Fig. 8.** Robust performance (RP) analysis

#### 4. Simulation Results

To investigate the behavior of the WRIM with the proposed  $H_{\infty}$  controller during unbalanced stator voltage, the typical diagram of the flywheel system integrated with wind farm shown in Fig.1 is constructed in MATLAB/SIMULINK using Simpower Systems, and the parameters are given in Table 1.

The WRIM driven flywheel storage system is controlled in order to smooth the power variation of the wind farm which is controlled to generate the optimal active power depending on the wind speed shown in Fig.9. The simulation results below were obtained for a desired grid active power of  $P_g = -8MW$ .

##### 4.1 Simulation results under normal conditions

The active power delivered to the grid by the wind farm is illustrated in Fig.10. As it can be seen, the wind active power varies according to the wind speed shown in Fig.9.

Figure 11 and Fig.12 show WRIM stator and rotor currents variations following the changes in wind speed as well. Figure 13 shows the rotor speed variation indicating that the flywheel system is charging and discharging to compensate the variation of wind power.

When active power is required by the power grid, the rotor speed is decreased, and the WRIM operates as a generator in order to inject the active power into the grid. When the rotor speed is increasing, the WRIM operates as a motor and consequently the active power is stored in the flywheel system.

Figure 14 shows the active power absorbed and delivered by the flywheel system. When the active power is positive, it indicates that the flywheel system absorbs active power from the wind farm. Whereas, negative power indicates that the flywheel system injects the active power into the grid. As a result, a constant active power is absorbed by the power grid as shown in Fig.15.

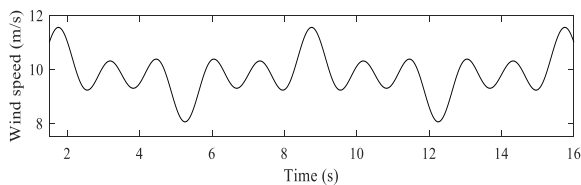


Fig. 9. Wind speed

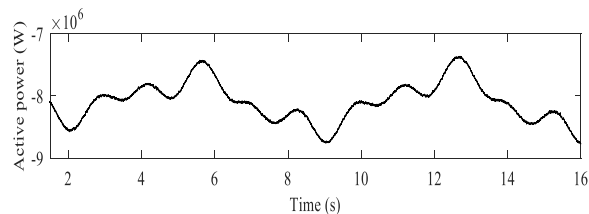


Fig. 10. Wind active power

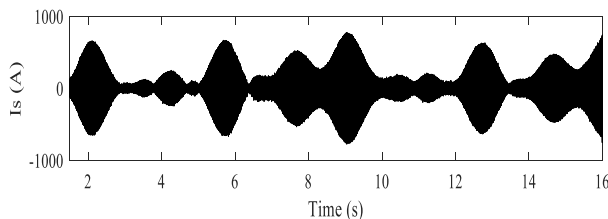


Fig. 11. WRIM stator currents

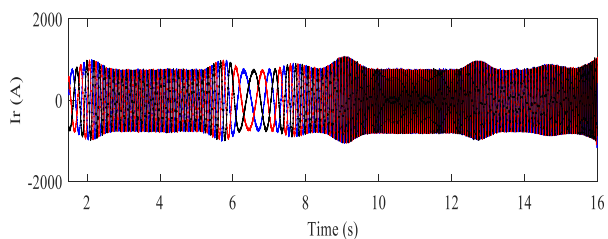


Fig. 12. WRIM rotor currents

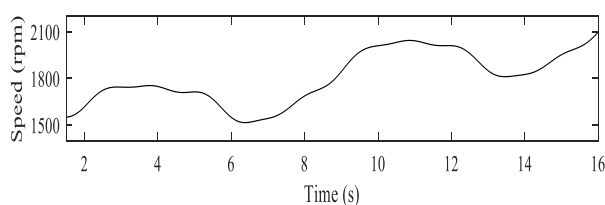


Fig. 13. WRIM rotor speed

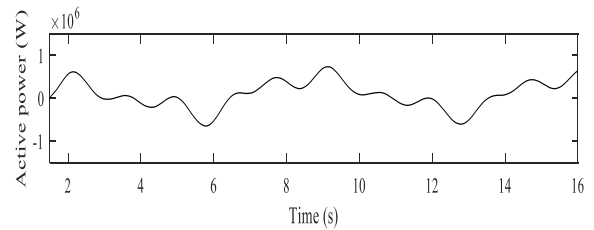


Fig. 14. WRIM active power

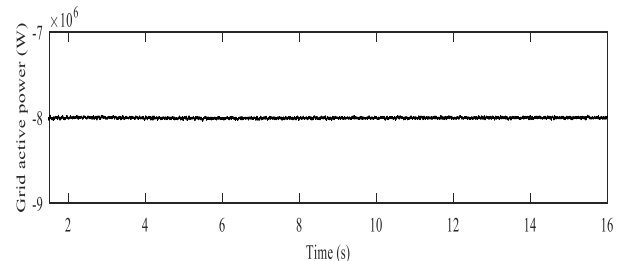


Fig. 15. Grid active power

#### 4.2 Simulation results under unbalanced stator voltage

To investigate the behavior of the WRIM driven FSS with the proposed  $H_\infty$  controller during unbalanced stator voltage, a single-phase fault with 30% dip depth is applied at phase A from  $t=2s$  to  $t=2.5s$ . Since the transient behavior of the flywheel system under stator voltage unbalance is the focus of this paper, the wind farm transient behavior is not shown. For the purpose of comparison, the PI and PIR controllers are also simulated under the same condition of stator voltage unbalance.

The PIR controller is expressed as [23]:

$$G_{PIR}(s) = k_p + \frac{k_i}{s} + \frac{2k_r w_c s}{s^2 + 2w_c s + w_r^2} \quad (17)$$

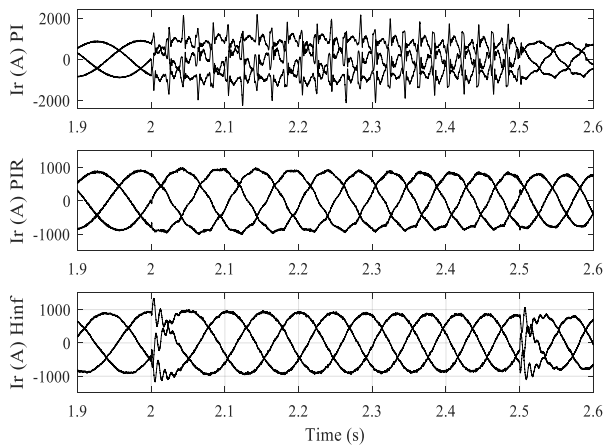
The parameters of the PIR controller are given in Table 3.

Figure 16 shows the comparison of the rotor current with different control cases. With classical PI controller, large negative sequence currents appear at the rotor side of the machine. This causes the rotor currents to rise to a high value which may damage the converters and results in the disconnection of the flywheel system from the grid. When the PIR and  $H_\infty$  controllers are applied to the rotor current control loop, the transient rotor currents remain under control. However, with the  $H_\infty$  controller the negative-sequence components in the rotor currents can be effectively suppressed.

Figure 17 shows the results of the active power of the WRIM driven flywheel storage system. The oscillations of the stator active power with classical PI controller are more severe than the PIR and  $H_\infty$  controllers. The active power oscillations are reduced both in the case of PIR and  $H_\infty$  controllers. However, the PIR controller presents better dynamic performance than the  $H_\infty$  controller.

**Table 3.** Parameters of the PIR controller

$k_p$	$k_i$	$k_r$	$w_c$	$w_r$
0.57	491.5	30	5	$200\pi$



**Fig. 16.** WRIM rotor currents under unbalanced stator voltage

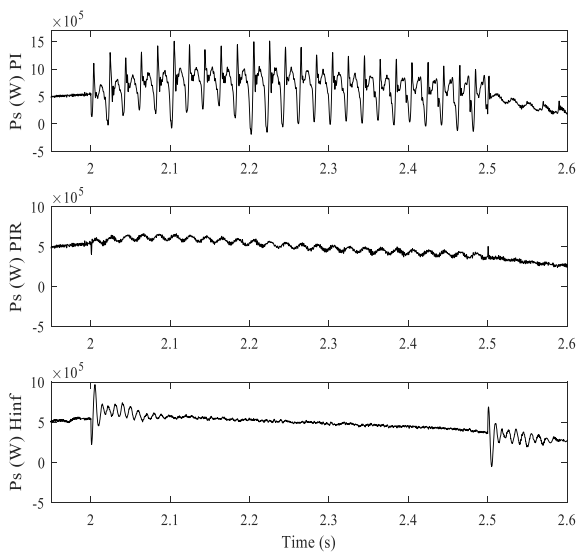


**Fig. 17.** Active power of the WRIM driven FSS under unbalanced stator voltage

**4.3 Simulation results under unbalanced stator voltage with machine parameter perturbation**

In the aim to test the robustness of the  $H_\infty$  controller against parameter uncertainties and for the same stator voltage unbalance, the values of  $L_m$ ,  $L_{\sigma s}$ ,  $L_{\sigma r}$  and  $R_r$  are increased by 50% of their nominal values.

The simulation results of the rotor currents with different control cases are shown in Fig.18. It is shown that that the performance of the proposed  $H_\infty$  controller tends to be

unaffected by the parameter perturbation and the rotor currents remain under control. While in the case of the conventional PI and PIR controllers, the performance control is highly degraded, which may affect the safe operation of the flywheel storage system.

Concerning the active power of the FSS based WRIM, the simulation results are shown in Fig.19, where it is found that the performance of the  $H_\infty$  controller remains unaffected to parameter perturbation. On the other hand, in the case of PI and PIR controllers, the performance control is influenced by parameter perturbation.

The above simulations show the effectiveness of the  $H_\infty$  controller in improving the performance of the WRIM based FSS under unbalanced stator voltage. Moreover, it is also seen that the proposed  $H_\infty$  controller guarantees the stability of the flywheel storage system based WRIM in the case of parameter uncertainties.

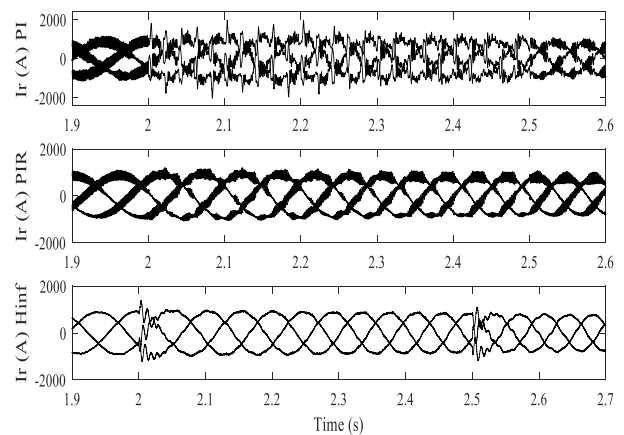


**Fig. 18.** WRIM rotor currents under unbalanced stator voltage with parameter perturbation

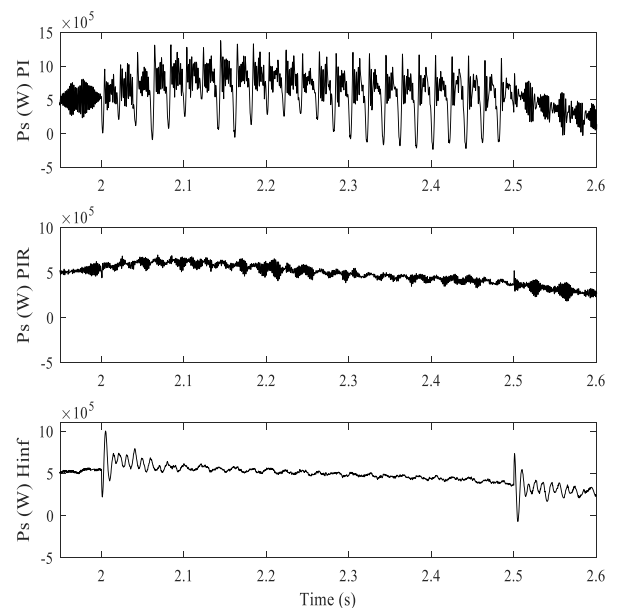


**Fig. 19.** Active power of the WRIM driven FSS under unbalanced stator voltage with parameter perturbation

## 5. Conclusion

In this work, a robust  $H_\infty$  controller was developed for the WRIM based FSS in order to guarantee the robustness under stator voltage unbalance and machine parameter uncertainties. The proposed  $H_\infty$  controller has been designed using mixed-sensitivity  $H_\infty$  control. The weights are selected in this design in order to suppress rotor currents oscillations resulting from negative sequence, and to guarantee the system RS and RP under stator voltage unbalance with parameter uncertainties.

Compared with the PI and PIR controllers, not only does the proposed  $H_\infty$  controller suppress rotor currents oscillations resulting from negative sequence, but also guarantees the robustness under parameter uncertainties. The simulation results demonstrate the effectiveness of the proposed  $H_\infty$  controller and confirm that the  $H_\infty$  control is a powerful tool for controlling flywheel storage systems under conditions of uncertainty and disturbances. On the other hand, the WRIM driven FSS with the proposed  $H_\infty$  controller can effectively ride through unbalanced stator voltage, improving thus wind energy penetration.

## References

- [1] A. Mir, N. Senroy, "Intelligently controlled flywheel storage for enhanced dynamic performance", *IEEE Trans. Sustain. Energy*, pp. 1-1, 2018.
- [2] S. Ghosh, S. Kamalasan, "An energy function-based optimal control strategy for output stabilization of integrated DFIG –flywheel energy storage system", *IEEE Trans. Smart Grid*, vol. 8, no.4, pp. 1922-1931, July 2017.
- [3] S. Belfedhal, E. Berkouk, "Modeling and Control of Wind Power Conversion System with a Flywheel Energy Storage System", *International journal of renewable energy research*, vol. 1, no.3, pp. 43-52, 2011.
- [4] F. Bouchafaa, I. Hamzaoui, A. Talha, "Control the Flywheel Storage System by Fuzzy Logic Associated with the Wind Generator", *International journal of renewable energy research*, vol. 2, no.4, pp. 723-729, 2012.
- [5] J. Yao, M. Yu, W. Gao, X. Zeng, "Frequency regulation control strategy for PMSG wind-power generation system with flywheel energy storage unit", *IET Renew. Power Gener.*, vol. 11, no.8, pp. 1082-1093, 2017.
- [6] N. Gayathri, N. Senroy, "Wind turbine with flywheel for improved power smoothing and LVRT", 2013 IEEE Power & Energy Society General Meeting, Canada, 21-25 July 2013.
- [7] B. Bolund, H. Bernhoff, M. Leijon, "Flywheel energy and power storage systems", *Renewable and Sustainable Energy Reviews*, vol. 11, no. 2, pp. 235-258, February 2007.
- [8] C. Ho, J. Wang, K. Hu, C. Liaw, "Development and operation control of a Switched-Reluctance Motor Driven Flywheel", *IEEE Trans. on Power Electron.*, vol. 34, no.1, pp. 526-537, January 2019.
- [9] E. Severson, R. Nilssen, T. Undeland, N. Mohan, "Magnetic Equivalent Circuit Modeling of the AC Homopolar Machine for Flywheel Energy Storage", *IEEE Trans. Energy Convers.*, vol. 30, no.4, pp. 1670-1678, December 2015.
- [10] S. Gurumurthy, V. Agarwal, A. Sharma, "Optimal energy harvesting from a high-speed brushless DC generator-based flywheel energy storage system", *IET Electr. Power App.*, vol. 7, no.9, pp. 693-700, November 2013.
- [11] H. Moghaddam, A. Vahedi, S. Ebrahimi, "Design Optimization of Transversely Laminated Synchronous Reluctance Machine for Flywheel Energy Storage System Using Response Surface Methodology", *IEEE Trans. Ind. Electron.*, vol. 64, no.12, pp. 9748-9757, December 2017.
- [12] S. K. Gagrai, S. Mishra, M. Singh, "Performance Analysis of Grid Integrated Doubly Fed Induction Generator for a Small Hydropower Plant", *International journal of renewable energy research*, vol. 8, no.4, pp. 2310-2323, December 2018.
- [13] M. Achglaf, C. Nichita, B. Dakyo, "Control Strategies Design for a Small-Scalle Wind Turbine with a Doubly Fed Induction Generator", 7<sup>th</sup> International Conference on Renewable Energy Research and Applications, Paris, France, 14-17 October 2018.
- [14] A. Broy, P. Tourou, C. Sourkounis, "Transient behaviour and active damping of vibrations in DFIG-based wind turbines during grid disturbances", 4<sup>th</sup> International Conference on Renewable Energy Research and Applications, Palermo, Italy, 22-25 November 2015.
- [15] A. Abdel-Khalil, A. Elserougi, A. Massoud, S. Ahmed, "Fault current contribution of medium voltage inverter and doubly-fed induction-machine-based flywheel energy storage system", *IEEE Trans. Sustain. Energy*, vol. 4, no.1, pp. 58-67, January 2013.
- [16] D. Kairous, R. Wamkeue, "DFIG-based fuzzy sliding-mode control of WECS with flywheel energy storage", *Elect. Power Syst. Res*, Vol. 93, pp. 16-23, December 2012.
- [17] L. Ran, D. Xiang, J. Kirtley, "Analysis of electromechanical interactions in a flywheel system with a doubly fed induction machine", *IEEE Trans. Ind. Appl.*, Vol. 47, No.3, pp. 1498-1506, May-June 2011.
- [18] S. muller, M. Deicke, R. De Doncker, "Doubly fed induction generator systems for wind turbines", *IEEE Ind. Appl. Mag.*, vol. 8, no.3, pp. 26-33, May-June 2002.
- [19] M. Doumi, I. Colak, A. G. Aissaoui, M. Abid, A. Tahour, "Robust MRAC for a wind turbine based on a doubly-fed induction generator", 6<sup>th</sup> International Conference on Renewable Energy Research and Applications, San Diego, CA, USA, 5-8 November 2017.

- [20] B. HAMANE, M. L. DOUMBIA, M. BOUHAMIDA, A. DRAOU, H. CHAOUI and M. BENGHANEM, "Comparative Study of PI, RST, Sliding Mode and Fuzzy Supervisory Controllers for DFIG based Wind Energy Conversion System", International journal of renewable energy research, vol. 5, no.4, pp. 1174-1185, 2015.
- [21] A. Lazrak, A. Abbou, M. Sidki, "Power control of DFIG based wind turbine during stator voltage drop", 3<sup>rd</sup> International Renewable and Sustainable Energy Conference (IRSEC), Marrakech, Morocco, 10-13 December 2015.
- [22] L. Xu, "Coordinated control of DFIG's rotor and grid side converters during network unbalance", IEEE Trans. on Power Electron., Vol. 23, No. 3, pp. 1041-1049, May 2008.
- [23] J. Hu, Y. He, L. Xu, B. Williams, "Improved control of DFIG systems during network unbalance using PI-R current regulators", IEEE Trans. Ind. Electron., Vol. 56, No. 2, pp. 439-451, February 2009.
- [24] A. Mirzakhani, R. Ghandehari, S. Davari, "A New DPC-based Control Algorithm for Improving the Power Quality of DFIG in Unbalance Grid Voltage Conditions", International journal of renewable energy research, vol. 8, no. 4, December, 2018.
- [25] R. V. Jacomini, J. Afleu, S. Filho, "Direct Power Control Strategy to Enhance the Dynamic Behavior of DFIG During Voltage Sag", 7<sup>th</sup> International Conference on Renewable Energy Research and Applications, Paris, France, 14-17 October 2018.
- [26] V. Phan, H. Lee, "Improved predictive current control for un- balanced stand-alone doubly-fed induction generator-based wind power systems", IET Electr. Power App., vol. 5, no.3, pp. 275-287, March 2011.
- [27] D. Sun, X. Wang, "Low-complexity model predictive direct power control for DFIG under both balanced and unbalanced grid conditions", IEEE Trans. Ind. Electron., Vol. 63, No. 8, pp. 5186-5196, August 2016.
- [28] L. Shang, J. Hu, "Sliding-mode-based direct power control of grid-connected wind-turbine-driven doubly fed induction generators under unbalanced grid voltage conditions", IEEE Trans. Energy Convers., vol. 27, no. 2, pp. 362-373, June 2012.
- [29] J. Chhor, P. Tourou, C. Sourkounis, « On advanced control strategies for DFIG-based wind energy conversion systems during voltage unbalance », 6<sup>th</sup> International Conference on Renewable Energy Research and Applications, San Diego, CA, USA, 5-8 November 2017.
- [30] Y. Wang, Q. Wu, R. Yang, G. Tao, Z. Liu, "H $\infty$  current damping control of DFIG based wind farm for sub-synchronous control interaction mitigation", Int. J. Electr. Power and Energy Syst., vol. 98, pp. 509-519, June 2018.
- [31] Y. Wang, Q. Wu, W. Gong, M. Gryning, "H $\infty$  robust current control for DFIG based wind turbine subject to grid voltage distortions", IEEE Trans. Sustain. Energy, Vol. 8, No. 2, pp. 816-825, April 2017.
- [32] D. McFarlane, K. Glover, "A loop-shaping design procedure using H $\infty$  synthesis", IEEE Trans. Autom. Control, Vol. 37, No. 6, pp. 759-769, June 1992.
- [33] A. Lazrak, A. Abbou, "Robust power control of DFIG based wind turbine without currents rotor sensor", 5th International Renewable and Sustainable Energy Conference (IRSEC), Tangier, Morocco, 4-7 December 2017.
- [34] S. Skogestad, I. Postlethwaite, Multivariable feedback control: analysis and design, 2nd ed., Wiley, 2005.
- [35] B. Muhando, R. Wies, "Nonlinear H $\infty$  constrained feedback control for grid-interactive WECS under high stochasticity", IEEE Trans. Energy Convers., vol. 26, no. 4, pp. 1000-1009, December 2011.
- [36] C. Belfedal, S. Gherbi, M. Sedraoui, S. Moreau, G. Champenois, T. Allaoui, M. Denai, "Robust control of doubly fed induction generator for stand-alone applications", Elect. Power Syst. Res., vol. 80, no.2, pp. 230-239, February 2010.
- [37] D. W. Novotny, T. A. Lipo, Vector control and dynamics of AC drives, Oxford University Press, 2000.
- [38] J. C. Doyle, K. Glover, P. P. Khargonekar, B. A. Francis, "State-space solutions to standard H/sub 2/ and H/sub infinity / control problems", IEEE Trans. Autom. Control Vol. 34, No. 8, pp. 831-847, 1989.